



**HAL**  
open science

## Selective area epitaxy of GaAs: the unintuitive role of feature size and pitch

Didem Dede, Frank Glas, Valerio Piazza, Nicholas Morgan, Martin Friedl, Lucas Güniat, Elif Nur Dayi, Akshay Balgarkashi, Vladimir Dubrovskii, Anna Fontcuberta I Morral

### ► To cite this version:

Didem Dede, Frank Glas, Valerio Piazza, Nicholas Morgan, Martin Friedl, et al.. Selective area epitaxy of GaAs: the unintuitive role of feature size and pitch. *Nanotechnology*, 2022, 33 (48), pp.485604. 10.1088/1361-6528/ac88d9 . hal-04261890

**HAL Id: hal-04261890**

**<https://hal.science/hal-04261890>**

Submitted on 27 Oct 2023

**HAL** is a multi-disciplinary open access archive for the deposit and dissemination of scientific research documents, whether they are published or not. The documents may come from teaching and research institutions in France or abroad, or from public or private research centers.

L'archive ouverte pluridisciplinaire **HAL**, est destinée au dépôt et à la diffusion de documents scientifiques de niveau recherche, publiés ou non, émanant des établissements d'enseignement et de recherche français ou étrangers, des laboratoires publics ou privés.

ACCEPTED MANUSCRIPT

# Selective area epitaxy of GaAs: the unintuitive role of feature size and pitch

To cite this article before publication: Didem Dede *et al* 2022 *Nanotechnology* in press <https://doi.org/10.1088/1361-6528/ac88d9>

## Manuscript version: Accepted Manuscript

Accepted Manuscript is “the version of the article accepted for publication including all changes made as a result of the peer review process, and which may also include the addition to the article by IOP Publishing of a header, an article ID, a cover sheet and/or an ‘Accepted Manuscript’ watermark, but excluding any other editing, typesetting or other changes made by IOP Publishing and/or its licensors”

This Accepted Manuscript is © 2022 IOP Publishing Ltd.

During the embargo period (the 12 month period from the publication of the Version of Record of this article), the Accepted Manuscript is fully protected by copyright and cannot be reused or reposted elsewhere.

As the Version of Record of this article is going to be / has been published on a subscription basis, this Accepted Manuscript is available for reuse under a CC BY-NC-ND 3.0 licence after the 12 month embargo period.

After the embargo period, everyone is permitted to use copy and redistribute this article for non-commercial purposes only, provided that they adhere to all the terms of the licence <https://creativecommons.org/licenses/by-nc-nd/3.0>

Although reasonable endeavours have been taken to obtain all necessary permissions from third parties to include their copyrighted content within this article, their full citation and copyright line may not be present in this Accepted Manuscript version. Before using any content from this article, please refer to the Version of Record on IOPscience once published for full citation and copyright details, as permissions will likely be required. All third party content is fully copyright protected, unless specifically stated otherwise in the figure caption in the Version of Record.

View the [article online](#) for updates and enhancements.

## Selective area epitaxy of GaAs: the unintuitive role of feature size and pitch

Didem Dede<sup>1</sup>, Frank Glas<sup>2</sup>, Valerio Piazza<sup>1</sup>, Nicholas Morgan<sup>1</sup>, Martin Friedl<sup>1</sup>, Lucas Güniat<sup>1</sup>, Elif Nur Dayi<sup>1</sup>, Akshay Balgarkashi<sup>1</sup>, Vladimir G. Dubrovski<sup>3</sup> and Anna Fontcuberta i Morral<sup>1,4</sup>

<sup>1</sup>Laboratory of Semiconductor Materials, Faculty of Engineering, Institute of Materials, EPFL, Lausanne, Switzerland

<sup>2</sup>Université Paris-Saclay, CNRS, Centre de Nanosciences et de Nanotechnologies, Palaiseau, France

<sup>3</sup>ITMO University, Saint Petersburg, Russia

<sup>4</sup>Faculty of Basic Sciences, Institute of Physics, EPFL, Lausanne, Switzerland

E-mail: [anna.fontcuberta@epfl.ch](mailto:anna.fontcuberta@epfl.ch)

**Abstract.** Selective area epitaxy (SAE) provides the path for scalable fabrication of semiconductor nanostructures in a device-compatible configuration. In the current paradigm, SAE is understood as localized epitaxy, and is modelled by combining planar and self-assembled nanowire growth mechanisms. Here we use GaAs SAE as a model system to provide a different perspective. First, we provide evidence of the significant impact of the annealing stage in the calculation of the growth rates. Then, by elucidating the effect of geometrical constraints on the growth of the semiconductor crystal, we demonstrate the role of adatom desorption and resorption beyond the direct-impingement and diffusion-limited regime. Our theoretical model explains the effect of these constraints on the growth, and in particular why the SAE growth rate is highly sensitive to the pattern geometry. Finally, the disagreement of the model at the largest pitch points to non-negligible multiple adatom recycling between patterned features. Overall, our findings point out the importance of considering adatom diffusion, adsorption and desorption dynamics in designing the SAE pattern to create pre-determined nanoscale structures across a wafer. These results are fundamental for the SAE process to become viable in the semiconductor industry.

Submitted to: *Nanotechnology*

## 1. Introduction

Selective area epitaxy (SAE) is an approach to grow crystal structures at desired locations on a wafer. It exploits a substrate covered with a patterned mask. Under certain growth conditions, crystals grow only at the exposed (non-covered) substrate surface.

Even though SAE was first proposed in the 1960s to fabricate III-V planar semiconductor structures [1–3], the interest towards this technique increased in the last decades thanks to two main advantages. First, SAE enables precise control over the morphology of the desired crystal, thus giving us flexibility in nanomaterial design.[4, 5] The morphology of the grown crystal can be engineered by changing the pattern geometry, growth parameters, and the crystal orientation of the host substrate.[6–8] The in-plane geometry of the crystal is mostly constrained by the pattern transferred to the mask. By simply altering the geometry of the apertures i.e., patterning circular holes, or rectangular slits, one can obtain quasi zero-, one- or two-dimensional structures including quantum dots, nanowires, nanofins, and nanomembranes.[6, 9–11] The out-of-plane geometry is strongly controlled by the growth parameters and the orientation of the host substrate. By exploiting the different wafer orientations and tuning the growth parameters, nanostructures with different facets and aspect ratios can be engineered.[8, 12, 13] The second advantage of SAE is scalability and flexibility. Having control over the position of the crystal growth paves the way towards wafer-scale fabrication of nanostructures. Compared to self-assembled growth, where randomness dominates, the epitaxial growth on patterned substrates results in structures with higher yield and uniformity.

Among different geometries, we are interested in the SAE of GaAs nanomembranes (NMs), as they may serve as templates for subsequent horizontal nanowire growth.[14, 15] Horizontal In-based nanowires (NWs) recently received significant attention due to their possible use in topological quantum computing.[16] By using SAE, scalable, high-quality branched NWs can be formed. Rather than directly growing these NWs on the host substrate, GaAs buffer layers or NMs can further enhance their structural properties.[17] First, NMs have high crystal-quality which makes them suitable templates for that purpose. Second, growing wires away from the substrate eliminates the migration of impurities that are present on the substrate due to processing.[18] Third, much smaller NWs can be obtained at the top facet of the NM, thus reducing the NW diameter with respect to the mask opening. Additionally, compared to NWs grown directly inside the openings, NWs grown on buffer layers show better transport properties.[17]

However, achieving a precise control over this process requires a deep understanding of the NM growth. Previously, the growth of NMs on (111)B GaAs substrates has been studied.[12, 19, 20] Such NMs are almost defect-free, and their shape is mostly kinetically driven, resulting in tunable aspect ratios. NWs grown on these membranes show an intermixing which is attributed to strain and the presence of high-index {311} facets.[14] On the contrary, when these NWs are grown on (100) membranes, an almost-pure InAs formation is observed. Full appreciation of thermodynamic factors and kinetic processes driving the NW growth is crucial to adjust the thickness or the geometry of the NWs.

In this work, we investigate the growth of NMs on (100) substrates. We start by examining the effect of annealing on patterned host substrates. Depending on the geometrical parameters, including width and pitch, we observe a significant difference in the desorption rate and a consistent variation of the surface roughness at the bottom of the slits. Compared to GaAs NMs grown on (111)B substrates, the growth on (100) is more thermodynamically driven, which results in more stable low-index facets. For slits along the  $\langle 01\bar{1} \rangle$  direction, we still observe the formation of {311} facets as an intermediate step, which then terminated by the formation of {111} side facets. The growth rate of GaAs in the slits also varies with the pattern geometry. We provide a dedicated theoretical model which highlights how adatom diffusion on the surface affects the GaAs growth rate in SAE. Both the experimental observations and the model converge towards the possibility to engineer the pattern geometry on the mask to locally control the growth kinetics. In this perspective, we believe that this study gives a broader insight into the growth mechanisms of NMs in SAE.

## 2. Experimental Results

A schematic representation of the patterned substrate and the configuration parameters is shown in Figure 1a. The growth areas consist of arrays of 10 parallel slits extending along the  $\langle 01\bar{1} \rangle$  direction. The shorter side of the slits is referred to as width (W) while the center-to-center distance and the side-to-side distance between two neighboring slits are referred to as pitch (P) and minimum distance (M), respectively. The nominal pitches chosen for this study are 500, 1000, 2000 and 4000 nm. For each nominal pitch, slits having 100, 160 and 240 nm nominal widths were examined. All slits are 50  $\mu\text{m}$  long. The difference between nominal and actual width values is due to the fabrication process, including the electron-beam lithography (EBL) patterning and the subsequent

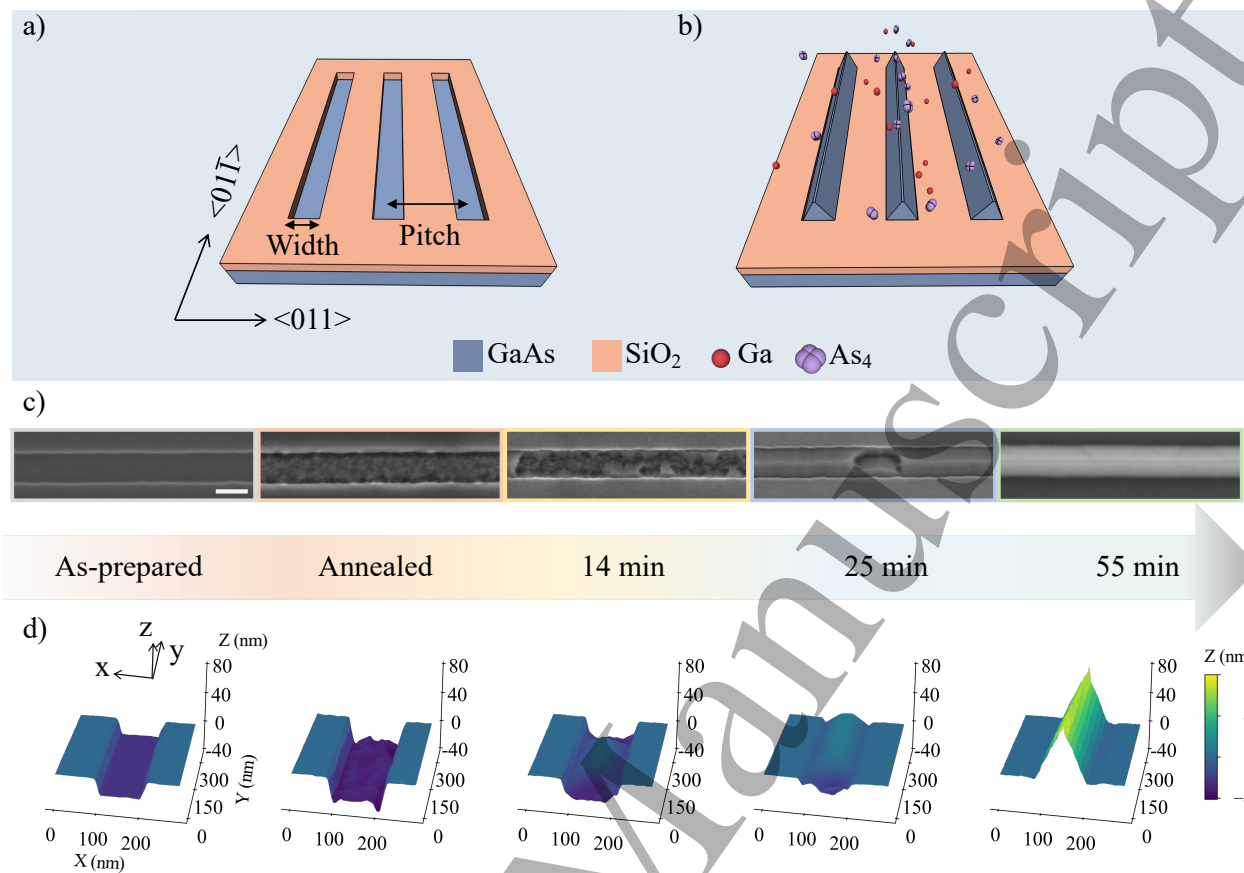


**Figure 1.** Schematic representation of as-patterned GaAs substrate prior to the growth (a) and after the growth of nanomembranes (b). Temporal evolution of GaAs nanomembranes: corresponding SEM (c) and AFM (d) images. Scale bar is 100 nm. Values in the AFM topography images are given in nanometers.

etching. Unless stated, the values given below will be the nominal ones. (see the Supporting information (SI), Figure S1)

Figure 1b sketches the shape of the fully grown GaAs NMs on (100) substrates. The NMs oriented along the <011̄> direction exhibit {111}A Ga-terminated side facets. Figure 1c contains representative scanning electron micrographs (SEMs) of the temporal evolution of a NM in a 100 nm nominal width slit with a 1000 nm pitch. The corresponding atomic force microscopy (AFM) images are shown in Figure 1d. Both SEM and AFM images indicate that annealing results in an increase in the surface roughness and depth of the slit. When the growth starts, small islands nucleate, and finally merge to form side facets belonging to the {311} family, which ultimately transition to the {111} facets, as shown further down. Even though all the slits follow a similar growth evolution, the temporal dependence strongly varies with their width and pitch. This dependence highlights the contributions of adatom desorption and diffusion to the NM formation. In other terms, this

observation suggests that the effective flux that each slit receives depends on the pattern dimensions, leading to relative delays in the growth evolution. In order to understand this mechanism, we fully characterized the dependence of the growth rate on the slit pitch and width.

We start by describing the stage prior to growth. This corresponds to the desorption of the native oxide under an  $As_2/As_4$  flux at 630°C. We note that in the literature this stage has not been well documented for SAE. Figure 2a shows the results of AFM measurements of 100 nm slits for pitches between 500 and 4000 nm after the desorption step. Both depth and roughness increase with the pitch. A similar trend is observed for wider slits (Figure S2). Figure 2b shows the average depth of the slits after the desorption step as a function of the pitch. The initial depth corresponds to a thickness of the mask oxide of about 22.5 nm. Note that in the figure, the increase in depth is given as negative assuming the top of the mask surface is at zero. In the annealing step the exposed surface of the substrate becomes rougher. This increase

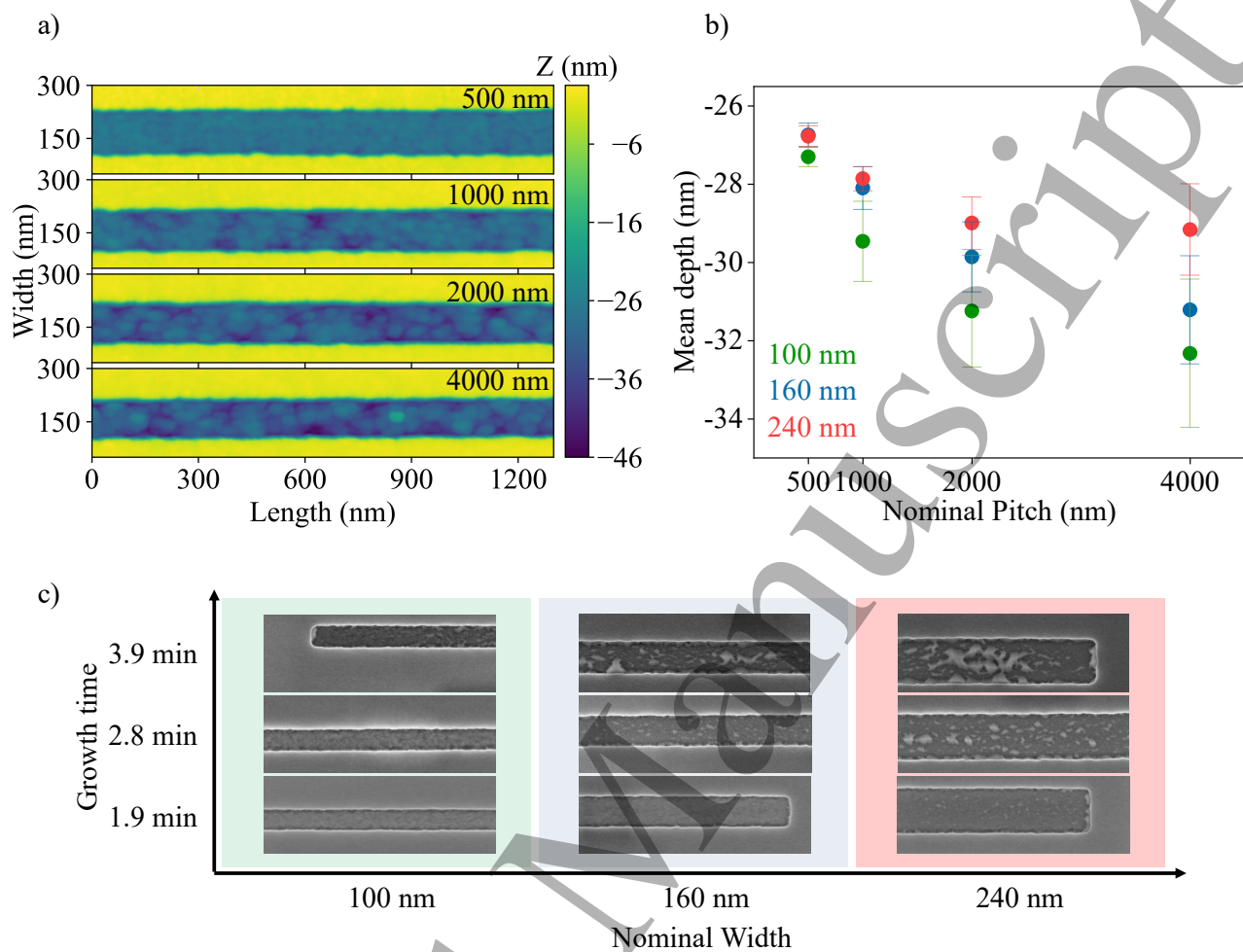


**Figure 2.** (a) Topography of annealed samples having 100 nm wide slits with different pitches. (b) The average depth measurement of various slits. We calculated the row averages along  $x$ , and the error bars show one standard deviation. (c) SEM micrographs of initial stages of the growth for three different widths and fixed 1000 nm pitch (c)

in the surface roughness in bare (100) GaAs substrates has been observed previously [21–24]. According to various studies, [25, 26] the native oxide is composed of oxides of gallium and arsenic, the latter being the more volatile [22]. After As oxides are desorbed at relatively low temperatures, additional time and temperature are needed to sublimate Ga oxides. More importantly, additional Ga supply from the GaAs substrate is necessary for these reactions to take place [27, 28]. This loss of material promotes the formation of pits on the surface. In our case, we observe an increase in the average depth from its initial value (22.5 nm). For a given width, the depth gradually increases with the pitch. This effect is more pronounced for narrower slits. In other words, the impact of the slit width becomes increasingly significant at larger slit pitches, suggesting that this phenomenon has a complex dependency on width and pitch. This desorption can be compensated

by an incoming  $As_2/As_4$  flux. We can expect that the effective As flux might have a dependence on dimensions. Furthermore, when an As atom desorbs, it leaves a Ga adatom behind which may diffuse on the surface before desorption or binding again with an incoming As atom. Obtaining a comprehensive picture of the mechanisms which define the complex interplay of width and pitch during the annealing step would require a large experimental effort and is beyond the purpose of this paper. In the context of this work, this analysis highlights that the impact of the pattern geometry is not limited to the GaAs growth and, thus, appears as a key factor for the correct description of SAE mechanisms. In addition, GaAs also desorbs from the region under the mask. As a result, before the growth starts, there is a significant increase in the slit depth and a slight increase in its width.

We now turn to the study of the GaAs growth

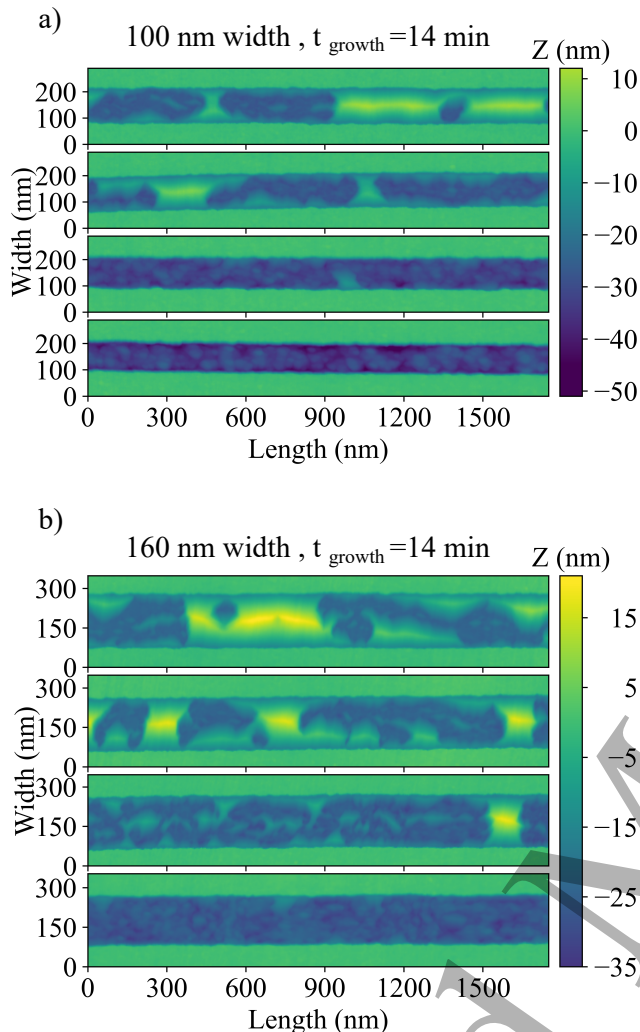


**Figure 3.** Pitch dependency of nanomembranes grown for 14 min having (a) 100 nm and (b) 160 nm widths. In each figure, pitch goes from 500 nm to 4000 nm from top to bottom.

inside the slits. For this, in addition to the arsenic flux, samples are exposed to a Ga flux for growth times between 2 and 55 minutes. Figure 2c shows SEMs of the structures obtained after 2 to 4 minutes of growth for three different slit widths. Initially, GaAs forms many nuclei which are distributed randomly inside the slit. No significant difference is observed between the edge and the center of the single slit. Growth of GaAs starts earlier for the 240 nm slit ( $<1.9$  min), followed by the 160 nm slit ( $<2.8$  min) and 100 nm slit ( $<3.9$  min). This prompted us to look into the growth evolution in more detail. Figures 3a and 3b show NMs grown for the same time of 14 min inside the 100 and 160 nm wide slits. For both nominal widths, the volume of GaAs grown in the slit decreases for increasing pitch. Hence, for a given slit width, the smallest pitches capture more material. At a fixed pitch, NMs develop at a faster rate

in wider slits.

It is worth noting that the NM faceting evolves during the growth. The temporal evolution of GaAs crystals formed in the slit having 240 nm width and 1000 nm pitch is shown in Figure 4a and 4b. Due to the low aspect ratios, facets can be identified by their inclination and orientation using AFM. In the initial stage, small GaAs crystals forming inside the slits exhibit  $\{311\}$  side facets exhibiting an inclination of  $25^\circ$  from the (100) surface. In the later stage, these nanocrystals merge and form a larger structure restricted by  $\{311\}$  facets which continues to grow until the NM emerges above the mask surface. Then, with increasing growth time (at 55 min for 240 nm width), the  $\{111\}$  facets start to form from the interface between the amorphous  $\text{SiO}_2$  mask and the membrane. The coexistence of  $\{311\}$  and  $\{111\}$  facets is further demonstrated in cross-section TEM images (Figures 4d and 4e). For fully grown membranes, we observe side facets inclined at  $54^\circ$  from the (100) surface, corresponding to the  $\{111\}$  crystal planes.

### 3. Theoretical Model and Discussion

Here, the experimental results are modeled, in view of gaining a better understanding of the microscopic processes occurring during SAE. The input of the model is the volume of GaAs grown inside each slit, calculated by averaging the height values inside the slit measured by AFM. The depth increase due to the loss of material during the annealing process is taken into account. We obtain the volume of GaAs grown per unit surface area. Figure 5a shows the geometrical parameters used in the model:  $W$  is the width of the slit and  $M$  is the minimum distance between the slits. Pitch,  $P$ , is equal to  $M+W$ . The  $x$  and  $y$  directions are normal and parallel to the slits, respectively. The net change in depth over time is given in Figure 5b for  $W=160$  nm and different pitches. The increase of the slope of the curves with respect to decreasing  $M$  indicates that the amount of material deposited is larger for smaller pitches. Figure 5c (solid dots) shows the dependence of the GaAs growth rate on width and pitch for all combinations of geometrical parameters investigated. Even though a fixed nominal growth rate was selected ( $0.3 \text{ \AA/s}$ ), the actual growth rate is lower than the nominal one, and moreover it is strongly affected by the geometrical constraints.[29]

One of the questions we want to answer is why the total volume of membrane grown in a slit in a given time decreases with increasing  $M$ . This seems non-intuitive if one considers that the amount of material collected from the vapor increases with  $M$ . At our growth temperature,  $\text{As}_4$  molecules are either adsorbed or desorbed from the surface. Therefore, our model

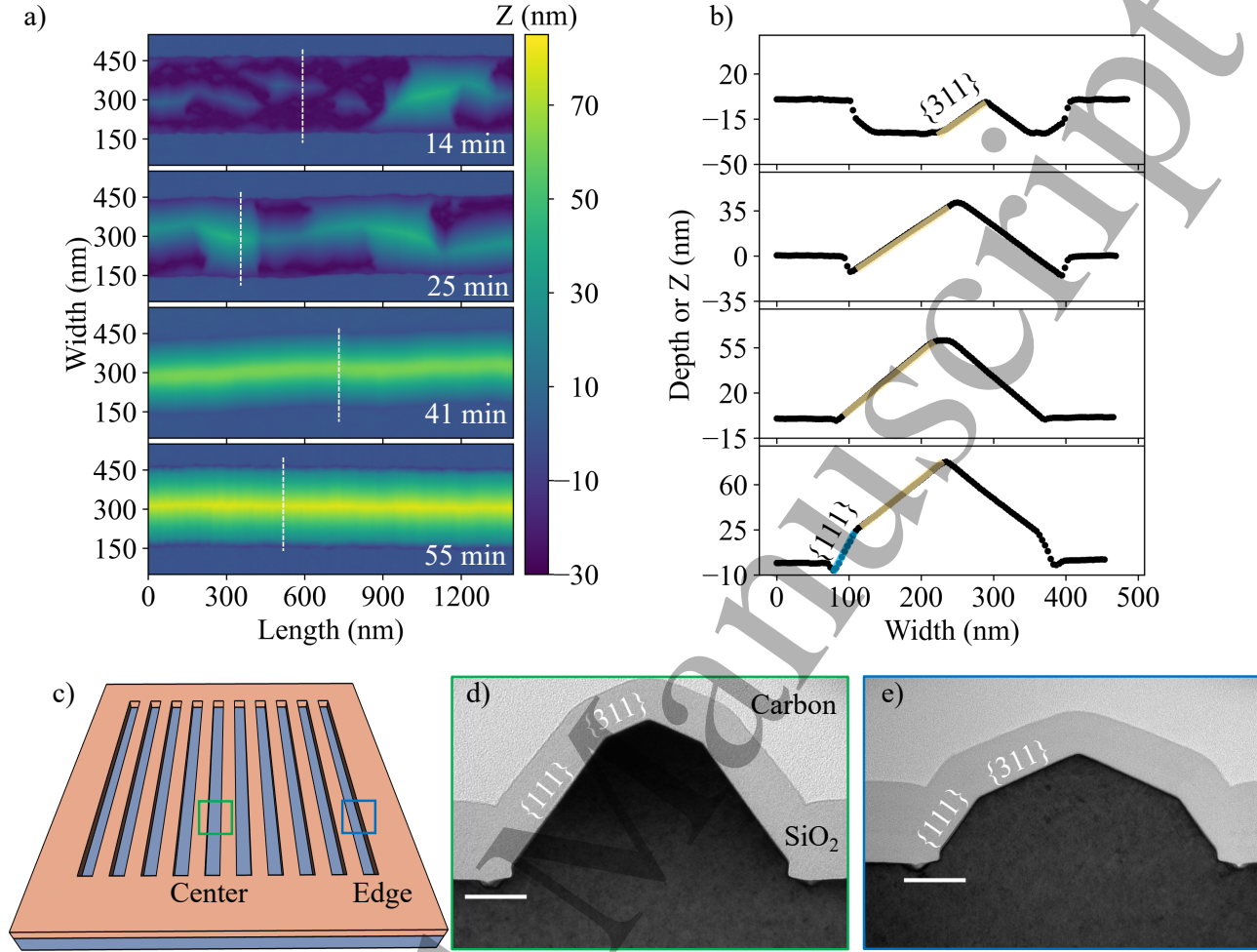


**Figure 4.** a) AFM contour plots of temporal evolution of 240 nm width slits having 1  $\mu\text{m}$  pitch. b) Cross sections that are drawn as white dashed lines in (a). c) Schematic diagram of slits showing locations at the edge and center. High resolution TEM images of 160 nm nominal width slits having 1  $\mu\text{m}$  pitch, d) center and e) edge slits respectively. Scale bar corresponds to 50 nm

considers only one adatom species, namely Ga, since it likely determines the growth rate. We model the local densities of the group III adatoms during growth in a stationary situation, with constant but non-uniform densities. Moreover, we assume that slits are long enough (50  $\mu\text{m}$ ) along  $y$  so that adatom densities depend only on  $x$ , and the growth rate is uniform over the width of the slit. We also assume that the adatom density is periodic along  $x$ , thereby neglecting edge effects that impact the slits at the periphery of the pattern. In Figure 4c-e, this edge effect is shown. Based on the height difference between structures, the variation in the growth rates can be seen. Please also check Figures S9 and S10. Subscripts  $i = m, s$  refer to mask and slit, respectively (we keep the term *slit* for the initial slit area throughout growth). The adatom densities are noted  $n_i$ .

We consider input from the vapor phase, surface

diffusion, desorption and incorporation to the solid of the adatoms. Input flux  $J$  (in  $\text{m}^{-2}\text{s}^{-1}$ ) is spatially uniform. Since we are considering the selective growth regime, the incorporation  $J_g$  (same unit) is zero on the mask. Surface diffusion is governed by the diffusion coefficients  $D_i$  (in  $\text{m}^2\text{s}^{-1}$ ) and characteristic times (in s) for desorption  $\tau_i$ . The corresponding diffusion lengths are  $\lambda_i = \sqrt{D_i\tau_i}$ . Therefore, adatom density (in  $\text{m}^{-2}$ ) on the mask ( $0 \leq x \leq M/2$ ) obeys equation:

$$J - \frac{n_m}{\tau_m} + D_m \frac{d^2 n_m}{dx^2} = 0 \quad (1)$$

The general solution of Eq. (1) is:

$$n_m(x) = A_m \cosh\left(\frac{x}{\lambda_m}\right) + B_m \sinh\left(\frac{x}{\lambda_m}\right) + J\tau_m \quad (2)$$

with  $A_m, B_m$  constants. Hence  $dn_m/dx = (A_m/\lambda_m) \sinh(x/\lambda_m) + (B_m/\lambda_m) \cosh(x/\lambda_m)$ . By

symmetry, the diffusion flux  $-D \, dn_m/dx$  cancels at the middle of the central mask band ( $x = 0$ ). Hence,  $B_m = 0$  and adatom density at the mask becomes

$$n_m(x) = A_m \cosh\left(\frac{x}{\lambda_m}\right) + J\tau_m \quad (3)$$

The adatom density in the first slit ( $M/2 \leq x \leq M/2 + W$ ) obeys equation:

$$J - \frac{n_s}{\tau_s} + D_s \frac{d^2 n_s}{dx^2} - J_g(x) = 0 \quad (4)$$

and it is symmetric around  $x = P/2$  (provided the slit is far enough from the edges of the array). We now assume that growth is uniform within the slit, so that  $J_g$  is a constant. Then, the solution of Eq. (4) is:

$$n_s(x) = A_s \cosh\left(\frac{x - \frac{P}{2}}{\lambda_s}\right) + (J - J_g)\tau_s \quad (5)$$

In order to determine the constants  $A_m$ ,  $A_s$ , we first write the continuity of the adatom current at the mask/slit boundary  $x = M/2$ :

$$-D_m \frac{dn_m}{dx} = -D_s \frac{dn_s}{dx} \quad (6)$$

The sign of this quantity indicates if the adatom flux is directed from mask to slit or from slit to mask. Hence:

$$D_m \frac{A_m}{\lambda_m} S_m = -D_s \frac{A_s}{\lambda_s} S_s \quad (7)$$

with  $S_m = \sinh[M/(2\lambda_m)]$ ,  $S_s = \sinh[W/(2\lambda_s)]$ .

A second boundary condition at the mask/slit interface is obtained via the transition rate theory [30] previously used in the field of nanowire growth [31–33]:

$$-D_m \frac{dn_m}{dx} \left(\frac{M}{2}\right) = k^+ n_m \left(\frac{M}{2}\right) - k^- n_s \left(\frac{M}{2}\right) \quad (8)$$

with  $k^+$  and  $k^-$  the rate constants (in  $\text{ms}^{-1}$ ) for the transfer of adatoms from mask to slit and slit to mask, respectively (Figure 5a) which, at variance with Ref.[31], we simply assume to be independent of adatom density [32, 33]. Recalling that the growth rate per unit area scales with  $J_g$ , from Eqs. (7) and (8), we find that  $J_g$  can be expressed as:

$$J_g = \delta J + \frac{FC_s A_s}{\tau_s} \quad (9)$$

where:

$$\delta = 1 - \frac{k^+ \tau_m}{k^- \tau_s} \quad (10)$$

$$F = 1 + \frac{S_s \lambda_s}{C_s k^- \tau_s} \left(1 + \frac{C_m k^+ \tau_m}{S_m \lambda_m}\right) \quad (11)$$

with  $C_m = \cosh[M/(2\lambda_m)]$ ,  $C_s = \cosh[W/(2\lambda_s)]$ . To find a solution and then compare the calculated growth rate (for a given set of system parameters) to our measurements, we need a second equation linking  $J_g$  and  $A_s$ , which can be obtained by relating growth rate  $J_g$  to adatom density  $n_s$ . Since  $J_g$  is fixed over the slit width whereas  $n_s$  is not, this relation must involve a global property of the adatom density. We tested a hypothesis in which the growth rate  $J_g$  is proportional to the maximum adatom density ( $n_s^{(m)}$ ) over the slit, namely  $J_g = \alpha n_s^{(m)}$ . From Eq.(5):

$$n_s^{(m)} = A_s + (J - J_g)\tau_s \quad (12)$$

Combining Eqs. (9) and (12), we finally find the growth rate corresponding to our hypothesis:

$$J_g^{(m)} = J \frac{\delta - FC_s}{1 - aFC_s} \quad (13)$$

where  $a = 1 + 1/(\alpha\tau_s)$ . Besides being proportional to the incident flux, the growth rate depends on five unknown parameters, namely  $k^+ \tau_m$ ,  $k^- \tau_s$ ,  $\lambda_m$ ,  $\lambda_s$  and  $\alpha\tau_s$ .

We modeled the data to find a single set of values of these five parameters that yield the best global fit between calculated growth rates and those extracted from the experiments (at all pitches and widths). In Figure 5c, we compare our experimental and calculated growth rates. Fits of similar quality can be obtained assuming different hypotheses on the adatom density (Figure S8). The model reproduces well the two main experimental trends: at fixed pitch, the growth rate increases with slit width, whereas at fixed slit width, it decreases when pitch (and hence the width of mask bands) increases. The latter result is striking, since one tends to believe that in SAE a wider mask band collects more source material and transfers it (if only partly) to the slit. But this intuitive conclusion must be overturned if, on the contrary, the transfer of material is predominantly from slit to mask. Examination of the fit results, and in particular of the sign of  $A_s$ , shows that this is actually the case. The adatoms desorb easily from the mask, which therefore acts as an efficient sink and this favors a transfer from the slits. On the other hand, the experimental growth rate becomes less sensitive to pitch when slit width increases, whereas our calculations predict the opposite. More precisely, the calculated values are in reasonable agreement with our experiments for pitches up to 2000 nm, but not for the largest pitch of 4000 nm. While the model predicts growth rate values similar to those at 2000 nm, indicating a sort of saturation, we measure a strongly reduced growth rate. There might be several reasons for this disagreement. First, our highly simplified model does not consider the 3D nature of the growth, with specific sticking coefficients

and desorption rates for each type of facet. This could be relevant since the NM shape changes from the beginning of growth till the formation of the complete (311) facets. Second, we supposed a stationary growth, despite the initial 3D growth mode, and even though the slit-mask boundary conditions will probably vary depending on the location of the boundary, below or above the mask level. To mitigate the impact of these two simplifications, we performed fits restricted to the latter growth period, where the NM is fully bounded by (311) facets of fixed area, which fully justifies the hypothesis of a growth rate uniform over slit width. The results were only marginally better. Finally, we assume that desorbed species leave the substrate, while they may remain there as adatoms and contribute to growth after transfer to neighboring slits. This effect may become negligible at very large pitches, a reason why the growth rate may strongly decrease.

#### 4. Conclusion

We have investigated and analyzed SAE from an uncommon perspective and demonstrated the effect of geometrical constraints on the homoepitaxial growth of GaAs NMs on (100) substrates. During initial annealing, after full oxide removal, further desorption from the substrate was found to depend on width and pitch of the slit openings. This dependency persists during growth, with higher growth rates for wider slits and narrower pitches. Since material transport on the surface is regulated by diffusion, a dependency on pitch is expected. However, in the standard picture of SAE, the diffusion of species collected by the mask toward the openings dominates and produces the reverse effect. To clarify this, we first studied in detail the development of the NMs, which starts with the random nucleation of small crystals with {311} facets. After merging inside the slits, the NMs display extended (311) and ( $\bar{3}\bar{1}\bar{1}$ ) facets, which finally transform into the more stable (111) and ( $1\bar{1}\bar{1}$ ) facets. We then developed a growth model incorporating adatom diffusion and desorption, which differ between mask and NM. The model explains the rather unintuitive decrease of the GaAs growth rate with increasing pitch by a transfer from slit and then NM to mask. The mask acts as a sink for diffusing species due to a high desorption rate. Overall, we showed that the geometrical constraints play an important role in SAE, with regards to both surface diffusion and crystal morphology. This stresses how crucial it is to consider the effect of width and pitch when designing wafer-scale devices.

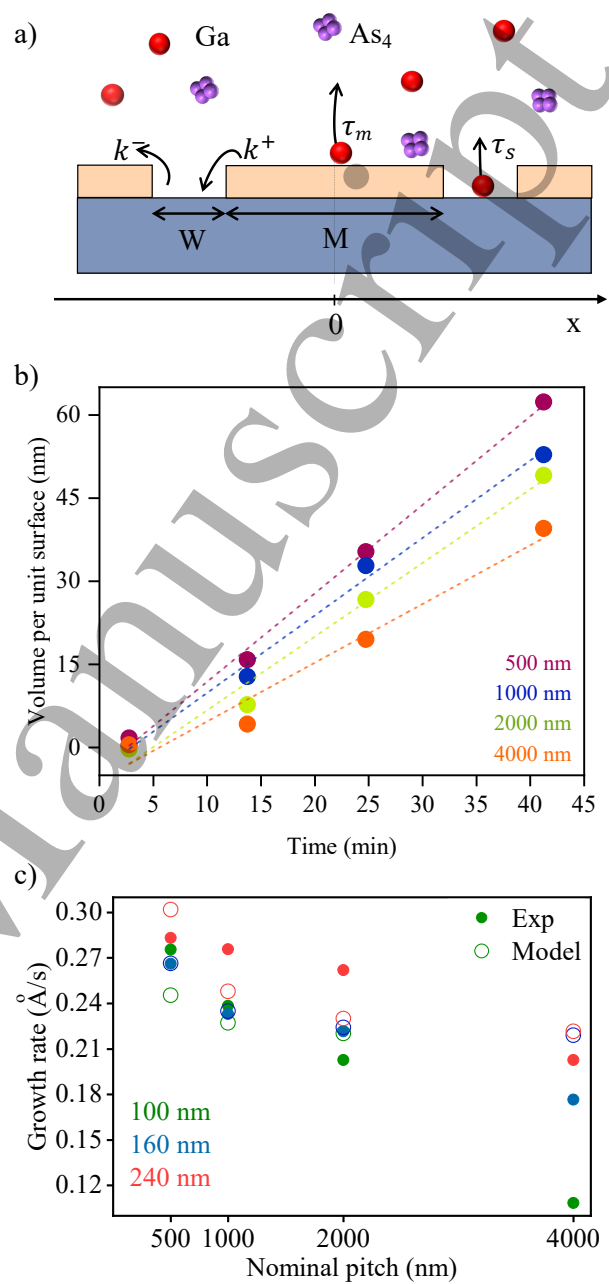


**Figure 5.** (a) Schematics of our system:  $\tau_m$  and  $\tau_s$  are the desorption times from the mask and from the slit,  $k^+$  and  $k^-$  are rate constants for transfer from mask to slit and slit to mask respectively. (b) Change in volume per unit area over time for slits of 160 nm nominal width having different pitch values. (c) Experimental growth rates (solid dots) and the outcome of our model (empty dots) assuming the growth rate is proportional to maximum adatom density, for all combination of pitch and slit width. Each point represent the slope of a linear fit of the variation of deposited thickness with time, as shown by dashed lines in (b).

## REFERENCES

## 5. Acknowledgments

The authors from EPFL acknowledge funding through the NCCR QSIT. Authors from EPFL further acknowledge funding from the Swiss NSF and Piaget. VGD gratefully acknowledges financial support of the research grant of St. Petersburg State University No. 75746688.

## 6. Methods

Semi insulating (100) GaAs wafers have been used to understand the effect of geometrical constraints on growth. To achieve selective growth, a 25 nm thick  $\text{SiO}_2$  mask was deposited by plasma-enhanced chemical vapor deposition (PECVD). Afterwards, the slit geometry was patterned by electron beam lithography (EBL) on ZEP positive resist and cold developed with n-amyl acetate. The desired pattern was then transferred to the mask by reactive ion etching with  $\text{CHF}_3/\text{SF}_6$  chemistry. Finally, the wafer was further etched with diluted HF to decrease the surface roughness of the oxide and remove the oxide residues from the GaAs slit surface. After this step, the surface roughness (RMS) of substrate is less than 0.5 nm as measured by AFM. The slits along  $\langle 01\bar{1} \rangle$  direction (parallel to substrate flat) have been further chosen to understand the morphological evolution of GaAs nanomembranes. As-prepared chips were introduced into the ultrahigh vacuum (UHV) environment of an MBE machine (DCA P600). The chips were initially degassed at 400°C (manipulator set temperature) for 2 hours in the degassing chamber to remove any organic molecules from the surface. Then the samples were transferred to the growth chamber. Prior to the growth, annealing was performed at 630°C. The samples were kept at a constant temperature for 10 minutes to remove all native oxide, which we estimate to be 3-4 nm thick. During this step, the  $\text{As}_4$  beam equivalent pressure (BEP) was  $6 \times 10^{-6}$  Torr. The GaAs growth has been performed with a 2D equivalent growth rate of 0.3 Å/s, with a V/III ratio of 80 which ensures selective growth at 630°C substrate temperature. In this study, we investigated the structures grown for 0 min (only annealing), 2 min, 5 min, 9 min, 14 min, 25 min and 55 min. Then we characterized the morphology and measured the grown volume using scanning electron microscopy and atom force microscopy.

## References

[1] Tausch F W and Lapierre A G 1965 *Journal of The Electrochemical Society* **112** 706 ISSN 00134651 URL <https://iopscience.iop.org/article/10.1149/1.2423670>

- [2] Shaw D W 1966 *Journal of The Electrochemical Society* **113** 904 ISSN 00134651 URL <https://iopscience.iop.org/article/10.1149/1.2424153>
- [3] Cho A Y and Ballamy W C 1975 *Journal of Applied Physics* **46** 783–785 ISSN 0021-8979, 1089-7550 URL <http://aip.scitation.org/doi/10.1063/1.321645>
- [4] Aseev P, Fursina A, Boekhout F, Krizek F, Sestoft J E, Borsoi F, Heedt S, Wang G, Binci L, Martí-Sánchez S, Swoboda T, Koops R, Uccelli E, Arbiol J, Krogstrup P, Kouwenhoven L P and Caroff P 2019 *Nano Letters* **19** 218–227 ISSN 1530-6984, 1530-6992 URL <https://pubs.acs.org/doi/10.1021/acs.nanolett.8b03733>
- [5] Yuan X, Pan D, Zhou Y, Zhang X, Peng K, Zhao B, Deng M, He J, Tan H H and Jagadish C 2021 *Applied Physics Reviews* **8** 021302 ISSN 1931-9401 URL <https://aip.scitation.org/doi/10.1063/5.0044706>
- [6] Seidl J, Gluschke J G, Yuan X, Tan H H, Jagadish C, Caroff P and Micolich A P 2021 *ACS Nano* **15** 7226–7236 ISSN 1936-0851, 1936-086X URL <https://pubs.acs.org/doi/10.1021/acsnano.1c00483>
- [7] Fonseka H A, Caroff P, Guo Y, Sanchez A M, Tan H H and Jagadish C 2019 *Nanoscale Research Letters* **14** 399 ISSN 1931-7573, 1556-276X URL <https://nanoscalereslett.springeropen.com/articles/10.1186/s11671-019-3177-6>
- [8] Lee J S, Choi S, Pendharkar M, Pennachio D J, Markman B, Seas M, Koelling S, Verheijen M A, Casparis L, Petersson K D, Petkovic I, Schaller V, Rodwell M J W, Marcus C M, Krogstrup P, Kouwenhoven L P, Bakkers E P A M and Palmström C J 2019 *Physical Review Materials* **3** ISSN 2475-9953 URL <https://link.aps.org/doi/10.1103/PhysRevMaterials.3.084606>
- [9] Birudavolu S, Nuntawong N, Balakrishnan G, Xin Y C, Huang S, Lee S C, Brueck S R J, Hains C P and Huffaker D L 2004 *Applied Physics Letters* **85** 2337–2339 ISSN 0003-6951, 1077-3118 URL <http://aip.scitation.org/doi/10.1063/1.1792792>
- [10] Güniat L, Caroff P and Fontcuberta i Morral A 2019 *Chemical Reviews* **119** 8958–8971 ISSN 0009-2665, 1520-6890 URL <http://pubs.acs.org/doi/10.1021/acs.chemrev.8b00649>
- [11] Vukajlovic-Plestina J, Kim W, Dubrovski V G, Tütüncüoğlu G, Lagier M, Potts H, Friedl M and Fontcuberta i Morral A 2017 *Nano Letters* **17** 4101–4108 ISSN 1530-6984, 1530-6992 URL <https://pubs.acs.org/doi/10.1021/acs.nanolett.7b00842>

## REFERENCES

10

- [12] Tutuncuoglu G, de la Mata M, Deiana D, Potts H, Matteini F, Arbiol J and Fontcuberta i Morral A 2015 *Nanoscale* **7** 19453–19460 ISSN 2040-3364, 2040-3372 URL <http://xlink.rsc.org/?DOI=C5NR04821D>
- [13] Escobar Steinvall S, Stutz E Z, Paul R, Zamani M, Dzade N Y, Piazza V, Friedl M, de Mestral V, Leran J B, Zamani R R and Fontcuberta i Morral A 2021 *Nanoscale Advances* **3** 326–332 ISSN 2516-0230 URL <http://xlink.rsc.org/?DOI=DONA00841A>
- [14] Friedl M, Cervený K, Weigele P, Tütüncüoğlu G, Martí-Sánchez S, Huang C, Patlatiuk T, Potts H, Sun Z, Hill M O, Güniat L, Kim W, Zamani M, Dubrovskii V G, Arbiol J, Lauhon L J, Zumbühl D M and Fontcuberta i Morral A 2018 *Nano Letters* **18** 2666–2671 ISSN 1530-6984, 1530-6992 URL <http://pubs.acs.org/doi/10.1021/acs.nanolett.8b00554>
- [15] Friedl M, Cervený K, Huang C, Dede D, Samani M, Hill M O, Morgan N, Kim W, Güniat L, Segura-Ruiz J, Lauhon L J, Zumbühl D M and Fontcuberta i Morral A 2020 *Nano Letters* **20** 3577–3584 ISSN 1530-6984, 1530-6992 URL <https://pubs.acs.org/doi/10.1021/acs.nanolett.0c00517>
- [16] Vaitiekėnas S, Whiticar A, Deng M T, Krizek F, Sestoft J, Palmstrøm C, Marti-Sanchez S, Arbiol J, Krogstrup P, Casparis L and Marcus C 2018 *Physical Review Letters* **121** ISSN 0031-9007, 1079-7114 URL <https://link.aps.org/doi/10.1103/PhysRevLett.121.147701>
- [17] Krizek F, Sestoft J E, Aseev P, Marti-Sanchez S, Vaitiekėnas S, Casparis L, Khan S A, Liu Y, Stankevič T, Whiticar A M, Fursina A, Boekhout F, Koops R, Uccelli E, Kouwenhoven L P, Marcus C M, Arbiol J and Krogstrup P 2018 *Physical Review Materials* **2** 093401 ISSN 2475-9953 URL <https://link.aps.org/doi/10.1103/PhysRevMaterials.2.093401>
- [18] Henini M 2013 *Molecular beam epitaxy from research to mass production* (Elsevier) pp 128–129 ISBN 978-0-12-387839-7
- [19] Albani M, Ghisalberti L, Bergamaschini R, Friedl M, Salvalaglio M, Voigt A, Montalenti F, Tütüncüoğlu G, Fontcuberta i Morral A and Miglio L 2018 *Physical Review Materials* **2** 093404 ISSN 2475-9953 URL <https://link.aps.org/doi/10.1103/PhysRevMaterials.2.093404>
- [20] Albani M, Bergamaschini R, Salvalaglio M, Voigt A, Miglio L and Montalenti F 2019 *physica status solidi (b)* **256** 1800518 ISSN 0370-1972, 1521-3951 URL <https://onlinelibrary.wiley.com/doi/abs/10.1002/pssb.201800518>
- [21] Ageev O A, Solodovnik M S, Balakirev S V, Mikhaylin I A and Eremenko M M 2016 *Journal of Physics: Conference Series* **741** 012012 ISSN 1742-6588, 1742-6596 URL <https://iopscience.iop.org/article/10.1088/1742-6596/741/1/012012>
- [22] Morota H and Adachi S 2009 *Journal of Applied Physics* **105** 043508 ISSN 0021-8979, 1089-7550 URL <http://aip.scitation.org/doi/10.1063/1.3078178>
- [23] Lee J J D, West K W, Baldwin K W and Pfeiffer L N 2012 *Journal of Crystal Growth* **356** 46–52 ISSN 0022-0248 URL <http://www.sciencedirect.com/science/article/pii/S0022024812004824>
- [24] Beznasyuk D V, Martí-Sánchez S, Kang J H, Tanta R, Rajpalke M, Stankevič T, Christensen A W, Spadaro M C, Bergamaschini R, Maka N N, Petersen C E N, Carrad D J, Jespersen T S, Arbiol J and Krogstrup P 2022 *Physical Review Materials* **6** 034602 ISSN 2475-9953 URL <https://link.aps.org/doi/10.1103/PhysRevMaterials.6.034602>
- [25] Guillén-Cervantes A, Rivera-Alvarez Z, López-López M, López-Luna E and Hernández-Calderón I 2000 *Thin Solid Films* **373** 159–163 ISSN 00406090 URL <https://linkinghub.elsevier.com/retrieve/pii/S0040609000011263>
- [26] Bastiman F, Hogg R, Skolnick M, Cullis A G and Hopkinson M 2010 *Journal of Physics: Conference Series* **209** 012066 ISSN 1742-6596 URL <https://iopscience.iop.org/article/10.1088/1742-6596/209/1/012066>
- [27] Vasquez R P, Lewis B F and Grunthaler F J 1983 *Applied Physics Letters* **42** 293–295 ISSN 0003-6951, 1077-3118 URL <http://aip.scitation.org/doi/10.1063/1.93884>
- [28] Pun A, Wang X, Durbin S and Zheng J 2007 *Thin Solid Films* **515** 4419–4422 ISSN 00406090 URL <https://linkinghub.elsevier.com/retrieve/pii/S0040609006009333>
- [29] Cachaza M E, Christensen A W, Beznasyuk D, Særkjær T, Madsen M H, Tanta R, Nagda G, Schuwalow S and Krogstrup P 2021 *Physical Review Materials* **5** 094601 ISSN 2475-9953 URL <https://link.aps.org/doi/10.1103/PhysRevMaterials.5.094601>
- [30] Hänggi P, Talkner P and Borkovec M 1990 *Reviews of Modern Physics* **62** 251–341 ISSN 0034-6861, 1539-0756 URL <https://link.aps.org/doi/10.1103/RevModPhys.62.251>
- [31] Krogstrup P, Jørgensen H I, Johnson E, Madsen M H, Sørensen C B, Morral A F i, Aagesen M,

## REFERENCES

11

- 1  
2 Nygård J and Glas F 2013 *Journal of Physics*  
3 *D: Applied Physics* **46** 313001 ISSN 0022-3727,  
4 1361-6463 URL [https://iopscience.iop.org/  
5 article/10.1088/0022-3727/46/31/313001](https://iopscience.iop.org/article/10.1088/0022-3727/46/31/313001)
- 6 [32] Dubrovskii V and Hervieu Y 2014 *Jour-*  
7 *nal of Crystal Growth* **401** 431–440 ISSN  
8 00220248 URL [https://linkinghub.elsevier.  
9 com/retrieve/pii/S0022024814000190](https://linkinghub.elsevier.com/retrieve/pii/S0022024814000190)
- 10 [33] Hervieu Y Y 2018 *Journal of Crystal*  
11 *Growth* **493** 1–7 ISSN 00220248 URL  
12 [https://linkinghub.elsevier.com/retrieve/  
13 pii/S0022024818301787](https://linkinghub.elsevier.com/retrieve/pii/S0022024818301787)  
14  
15  
16  
17  
18  
19  
20  
21  
22  
23  
24  
25  
26  
27  
28  
29  
30  
31  
32  
33  
34  
35  
36  
37  
38  
39  
40  
41  
42  
43  
44  
45  
46  
47  
48  
49  
50  
51  
52  
53  
54  
55  
56  
57  
58  
59  
60

Accepted Manuscript